Physical Mechanisms Driving Oxygen Subduction in the Global Ocean

Esther Portela, Nicolas Kolodziejczyk, Clément Vic, Virginie Thierry

HAL Id: insu-03683223

https://insu.hal.science/insu-03683223

Submitted on 1 Jun 2022

Geophysical Research Letters

Key Points:
- Up to 70% of the global oxygen uptake occurs during Mode Water subduction, driven by lateral induction and vertical velocity
- Oxygen diffusion, despite large uncertainties, is likely to play an important role in the global oxygen uptake
- Total oxygen subduction is driven by the mass flux, with little contribution of the latitudinal variability of oxygen concentration

Supporting Information:
- Supporting Information S1

Correspondence to:
E. Portela,
eportelanh@gmail.com

Physical Mechanisms Driving Oxygen Subduction in the Global Ocean

Esther Portela[1] [ID], **Nicolas Kolodziejczyk[1]** [ID], **Clément Vic[1]** [ID], and **Virginie Thierry[1]** [ID]

[1]Université Brest, CNRS, IRD, Ifremer, Laboratoire d'Océanographie Physique et Spatiale (LOPS), Plouzané, France

Abstract Future changes in subduction are suspected to be critical for the ocean deoxygenation predicted by climate models over the 21st century. However, the drivers of global oxygen subduction have not been fully described or quantified. Here, we address the physical mechanisms responsible for the oxygen transport across the late-winter mixed layer base and their relation with water mass formation. Up to 70% of the global oxygen uptake takes place during Mode Water subduction mostly in the Southern Ocean and the North Atlantic. Te driving mechanisms are (i) the combination of strong currents with large mixed-layer-depth gradients at localized hot spots and (ii) the wind-driven vertical velocity within the subtropical gyres. Oxygen diffusion, despite being underestimated in this study, is likely to play an important role in the global ocean oxygenation. The physical mass flux dominates the total oxygen subduction while the oxygen solubility plays a minor role in its modulation.

1. Introduction

A deoxygenation trend has been observed over the past decades in the global ocean, and it is predicted by climate models to increase over this century (Bopp et al., 2002, 2013; Helm et al., 2011; Ito et al., 2017; Keeling & Garcia, 2002; Keeling et al., 2010; Oschlies et al., 2018; Schmidtko et al., 2017). This decrease in the global ocean oxygen concentration ($[O_2]$) has been attributed to the warming climate operating directly via the reduced oxygen solubility and indirectly by an increased stratification and changes in respiration and ventilation (Oschlies et al., 2018; Schmidtko et al., 2017). Ocean ventilation refers to the combination of processes by which the surface waters that have been recently in contact with the atmosphere are injected into the ocean interior (kinematic and diffusive subduction) (Cushman-Roisin, 1987; Marshall et al., 1993; Qiu & Huang, 1995) and transported away from their sources (interior circulation and mixing) (Luyten et al., 1983; Naveira Garabato et al., 2017).

Reduced ventilation has been proposed as the main mechanism driving the ongoing global oxygen loss (Helm et al., 2011; Keeling & Garcia, 2002; Keeling et al., 2010; Long et al., 2016). However, the different ventilation processes have not been fully unraveled or quantified. On decadal timescales, the strongest negative oxygen trends have been detected in the least-ventilated regions with an associated expansion of the oxygen minimum zones (Helm et al., 2011; Schmidtko et al., 2017; Stramma et al., 2008), while newly subducted water masses do not show a detectable deoxygenation signal (Helm et al., 2011; Oschlies et al., 2018; Schmidtko et al., 2017). These patterns suggest that oxygen loss over the past decades is consistent with a reduced interior transport and the overturning circulation slowdown (Brandt et al., 2015; Oschlies et al., 2018; Schmidtko et al., 2017). In contrast, a recent climate model simulation has shown reduced subduction to be a major driver of long-term oxygen loss, suggesting that changes in location and intensity of subduction are critical to understanding the long-term deoxygenation (Couespel et al., 2019).

In the context of climate change, given the importance of the subduction process for the present and future of the oceanic oxygen content, it is crucial to understanding and quantify the global oxygen subduction (S^{ox}). During water mass formation, at high latitudes, oxygen is subducted into the ocean interior, while oxygen is released back into the mixed layer (ML) in zones of strong upwelling (Liu & Huang, 2012). In this study, we delve into the relative contributions of the physical mechanisms driving the oxygen uptake and release by the ocean interior. We also focus on the mechanisms setting the relationship between these ventilation regions and the associated water masses, which is still poorly understood at global scales.
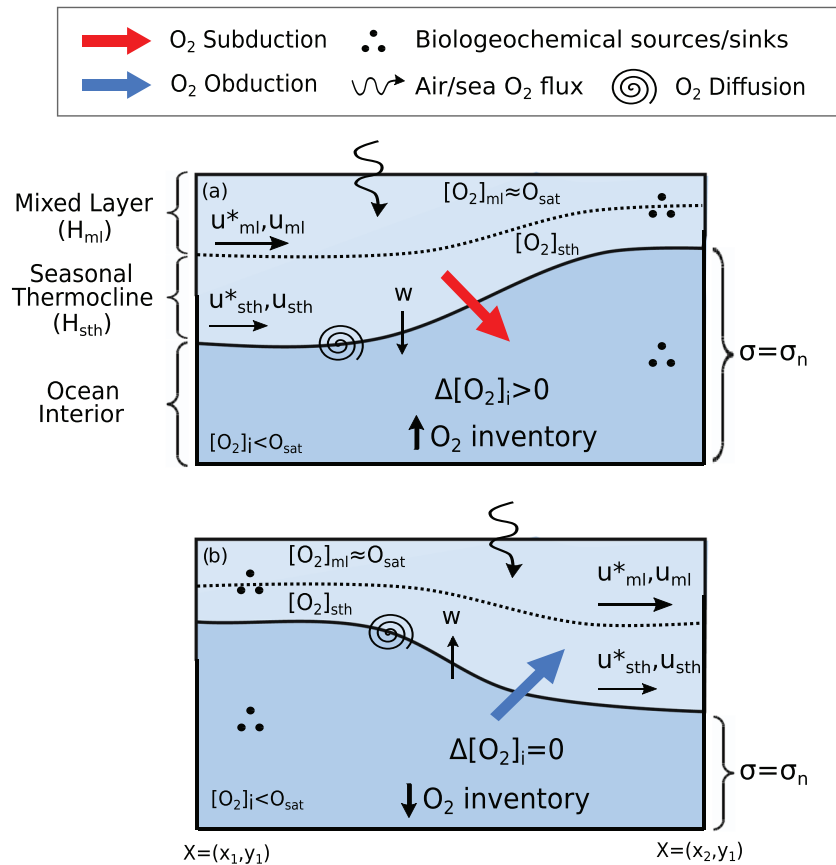
Figure 1. Schematic of the elements implied in (a) S^{ox} and (b) O^{ox} and their effect on the oxygen inventory and $[O_2]_i$ within a seawater volume confined between the steady late winter ML base and a variable density surface ($\sigma = \sigma_n$). Subduction brings oxygenated waters into the ocean interior, which increases the interior oxygen inventory and $[O_2]_i$. In contrast, obduction reduces the interior oxygen inventory due to the net volume loss, but $[O_2]_i$ remains invariable. S^{ox} is computed by taking into account the different geostrophic (U) and eddy (U^*) velocity within the mixed layer (*ml*) and the seasonal thermocline (*sth*).

2. Key Concepts on Oxygen Subduction

There are three competing processes driving the global ocean oxygen inventory: (i) the air/sea transfer tied to oxygen solubility (Koelling et al., 2017), mainly controlled by the seawater temperature; (ii) the S^{ox} that carries the oxygen-rich surface waters to the ocean interior (Cushman-Roisin, 1987; Marshall et al., 1993); and (iii) the biological respiration and remineralization (Resplandy, 2018; Wyrtki, 1965). Within the ML, $[O_2]$ is, to first order, in equilibrium with the atmosphere and therefore close to 100% saturation (O_{sat}), deviations from saturation are usually found in deep convection zones (Koelling et al., 2017).

In Figure 1 we illustrate the oxygen subduction/obduction process and their effect on interior $[O_2]$ ($[O_2]_i$) and the oxygen inventory. The ML acts as a buffer between the atmosphere and the ocean interior. Oxygen obduction (O^{ox}) is defined here as the opposite of subduction, that is, the oxygen flux from the permanent thermocline through the steady, late winter ML base into the seasonal thermocline/ML (Kwon et al., 2016; Marshall et al., 1993; Sallée et al., 2010, 2012). To isolate the subduction effect, for simplicity, in this conceptual schematic, we set a steady oxygen solubility in the ML and a constant respiration in time and space. While biogeochemical processes are important to modulate $[O_2]$ in certain regions (Richardson & Bendtsen, 2017), they are beyond the scope of this study.

Putting aside the effect of biogeochemical processes, S^{ox} increases the oxygen inventory within a given volume confined between the late winter ML base and a variable isopycnal surface (σ_n). This is because

the volume increases due to the positive mass flux and because of the uptake of oxygenated waters with $[O_2] \approx O_{sat}$ by the ocean interior. Since O_{sat} is usually higher than $[O_2]_i$, this process also increases $[O_2]_i$.

In an obductive location, the oxygen inventory decreases due to the negative mass flux. However, this flux alone will not change $[O_2]$ of the given volume ($\Delta[O_2]_i = 0$; Figure 1b). $[O_2]$ in the ML ($[O_2]_{ml}$) decreases due to the mixing of nearly saturated waters with interior waters with lower $[O_2]$. However, due to the air-sea equilibrium, the $[O_2]_{ml}$ rapidly resaturates (few days for a ML of 50 m, (Gruber et al., 2001)). Note that oxygen diffusion can take place in a net obductive location where it would increase the local $[O_2]_i$. However, the kinematic mass and oxygen flux to the ML overwhelms this effect. In the global ocean mass must be conserved, and the obduction and subduction mass flux must compensate each other. This implies that S^{ox} is the only dynamical mechanism able to increase the global $[O_2]_i$. The subsequent water mass mixing and spreading do not change the global oxygen inventory, but they drive the oxygen distribution over the entire ocean at interannual to decadal timescales (Joos et al., 2003).

3. Methods

3.1. Oxygen Subduction Computation

While the ML depth varies seasonally with the resulting entrainment/detrainment of water, permanent subduction (in contrast with the instantaneous subduction first described by Cushman-Roisin, 1987) accounts for the fraction of water that has irreversibly entered the permanent thermocline across the steady late-winter ML base (H_{max}) (Donners et al., 2005; Marshall et al., 1993). This permanent S^{ox} is determined by the mass flux across H_{max} carrying the in situ oxygen (kinematic subduction) and by the turbulent oxygen diffusion due to the difference in $[O_2]$ in the ML/seasonal thermocline and the ocean interior. Following Sallée et al. (2012), S^{ox} (positive into the ocean interior) is expressed as follows :

$$\overline{S^{ox}} = \underbrace{\overline{[O_2]} \cdot \overline{U} \cdot \nabla \overline{H_{max}}}_{\text{Lateral induction}} + \underbrace{\overline{[O_2]} \cdot \nabla(\overline{U^* H_{max}})}_{\text{Eddy -induced}} + \underbrace{\overline{[O_2]} \cdot \overline{w}}_{\text{Vertical}} + \underbrace{k_v \cdot \nabla_v \overline{[O_2]} + k_l \cdot \nabla \overline{[O_2]} \cdot \nabla \overline{H_{max}}}_{\text{Diffusion}} \tag{1}$$

where U and U^* are, respectively, the horizontal mean and bolus velocity fields; w is the vertical velocity; and ∇ is the horizontal divergence operator. U^* represents the advective contribution of unresolved eddies (Forget et al., 2015) parametrized following Gent and McWilliams (1990). Vertical diffusion in the ocean interior is mainly driven by turbulent mixing induced by the breaking of internal tides (Munk & Wunsch, 1998). Hence, we use a geographically variable vertical diffusion coefficient (k_v) based on a parametrization of tidally driven mixing (de Lavergne et al., 2020). k_v is determined at the base of the ML as $k_v = 0.2\varepsilon/N^2$ (Osborn, 1980), where ε is the turbulent energy dissipation and N^2 is the buoyancy frequency.

Based on previous studies, the lateral diffusion coefficient is set to be $k_l = 10^3$ m^2 s^{-1} (Forget et al., 2015; Köhl et al., 2007). However, this coefficient is spatially variable (Abernathey & Marshall, 2013; Klocker & Abernathey, 2014) and uncertain as it is based on parametrizations that depend on the data set resolution. To discuss the potential role of lateral diffusion on the global S^{ox}, we computed diffusion with the lower ($k_l = 10^2$ m^2 s^{-1}) and upper ($k_l = 10^4$ m^2 s^{-1}) limits for k_l as found in the literature (Forget et al., 2015).

S^{ox} was computed by considering $H_{max} = H_{ml} + H_{sth}$ (Sallée et al., 2010), where subscripts ml and sth denote the seasonal ML and the seasonal thermocline, respectively (Figure 1). The decomposition of the lateral induction term in Equation 1 (similarly applied to the eddy-induced term) becomes

$$\overline{[O_2]} \cdot \overline{U} \cdot \nabla \overline{H} = \overline{[O_2]}_{ml} \cdot \overline{U_{ml}} \cdot \nabla \overline{H_{ml}} + \overline{[O_2]}_{sth} \cdot \overline{U_{sth}} \cdot \nabla \overline{H_{sth}}. \tag{2}$$

This method takes into account the seasonal variation of $[O_2]$ and the different U and U^* in the two layers whose respective thickness vary seasonally. The uncertainty associated with the sparse oxygen sampling and the interannual variability of oxygen and subduction is discussed in the supporting information

(Figures S1 and S2); our analysis suggests that the scarcity of oxygen data could be the main source of uncertainty.

3.2. Data

All the physical variables (U, U^*, temperature, and salinity) were obtained from the state estimate produced by the consortium for Estimating the Circulation and Climate of the Ocean (ECCOv4 r3) (Fukumori et al., 2017). We have used climatological monthly mean values averaged over 1992–2015 with horizontal resolution of 0.5° × 0.5°. The vertical grid spacing increases from 10 m near the surface to 457 m near the ocean bottom.

To validate the results obtained with ECCOv4, we computed the kinematic S^{ox} using the gridded Argo product In situ Analysis System (ISAS15) (Gaillard et al., 2016; Kolodziejczyk et al., 2017). The resulting fields are available in the supporting information and show a good agreement (Figure S3). The main differences are due to the small-scale structures that arise in the data-based computation. These structures could be a result of the noisy fields, or they could arise as a product of the finer mesh in ISAS15. However, the main hot spots and global features are well represented by both products with similar magnitude.

The monthly climatology of dissolved oxygen data was obtained from the World Ocean Atlas 2018 (WOA18) (Garcia et al., 2019), which provides statistical and objectively analyzed data fields at 1° × 1° resolution. All oxygen data used in WOA18 are bottle-based and have been obtained through the Winkler titration method. The oxygen field was interpolated onto the ECCOv4 grid.

Here, we examine mean S^{ox} from monthly climatological fields (overbars in Equation 1). Note that oxygen monthly climatology in WOA18 is provided at 57 depth levels between 0 and 1,500 m. Below that depth, we have used the annual climatology that is provided until 5,500 m depth. We assume that below 1,500, the seasonal variability in the oxygen climatology is negligible.

There are some characteristics of the WOA18 data set that introduce a degree of uncertainty. (i) The WOA18 climatology covers the period 1955–2017 while ECCOv4 outputs are provided between 1992 and 2015. (ii) WOA18 oxygen data contain only bottle samples. This implies a reduced vertical resolution and vertical oxygen gradient. (iii) The use of interpolated fields smooths the oxygen gradients in comparison with raw profiles. The last two characteristics of the dataset can lead to an underestimation of the vertical oxygen diffusion term. Other sources of uncertainty as those derived from the uneven oxygen sampling or the unresolved timescales are further discussed in the supporting information (section S1: Figures S1 and S2; Equation S2).

4. Results

4.1. Geographical Distribution of Oxygen Subduction

The largest oxygen fluxes into the thermocline are located (i) in the Southern Ocean (37%), with maximum to the east of Drake Passage, and (ii) in the northern North Atlantic (30%), particularly in Labrador, Irminger, and Nordic Seas (Liu & Huang, 2012). The Barents Sea constitutes an isolated hot spot of oxygen uptake (Figure 2e) within the Arctic Ocean. In addition, we identify weaker, but homogeneous subductive regions shaped by the subtropical gyres in every ocean basin. The majority of the O^{ox} occurs in three regions: around 45% takes place in the Southern Ocean, around 22% in the subtropical-subpolar North Atlantic, and 14% in the equatorial strip.

S^{ox} is globally shaped by lateral induction (Figure 2a), the component with the highest magnitude located in well-defined hot spots. Nonetheless, lateral induction produces a global net deoxygenation (−142 Tmol year^{-1}), which is driven by large MLD gradients in combination with strong regional currents (Figure S4b). Lateral induction is maximum in the northern North Atlantic (Labrador and Irminger and Nordic seas) and in the Southern Ocean. The latter is driven by the intense Antarctic Circumpolar Current (ACC) (Figure S4b). In the subtropical-subpolar North Atlantic, the Gulf Stream and the North Atlantic Current act as dynamical barriers; weak oxygen uptake occurs to the southeast, while intense O^{ox} extends northeastward from the Florida Strait to the Norwegian Sea (Figure 2d) (Marshall et al., 1993; Qiu & Huang, 1995).
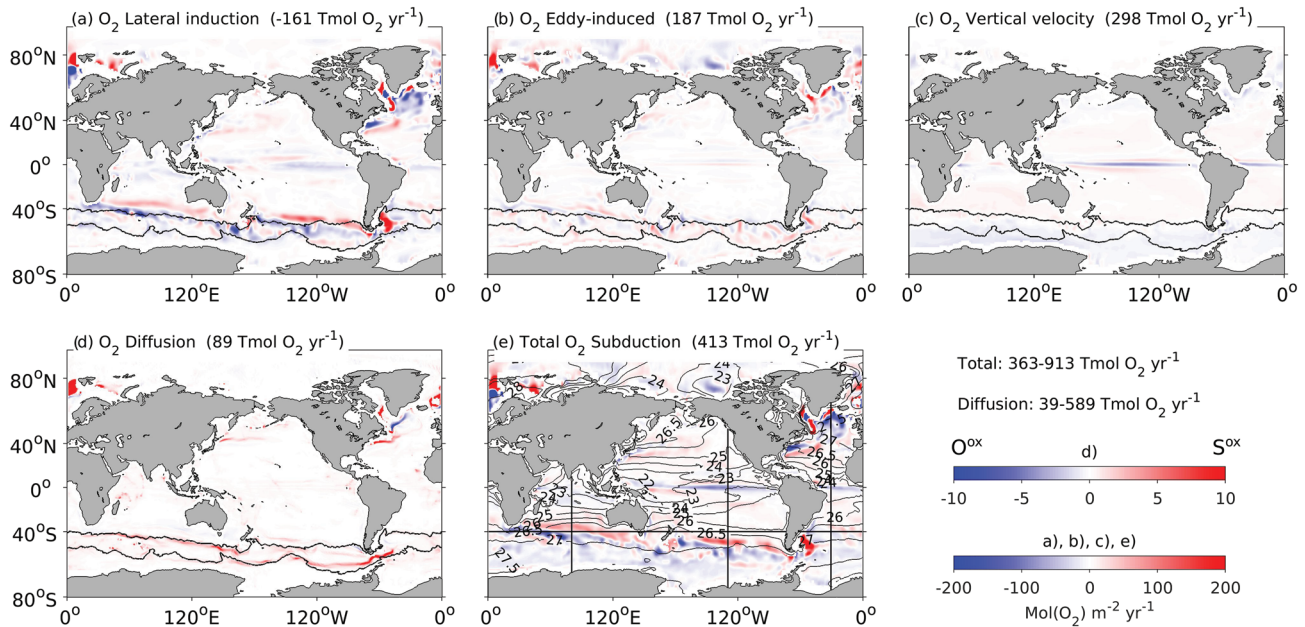
Figure 2. Spatial distribution of S^{ox} and its components. (a) Lateral induction, (b) eddy-induced, (c) vertical velocity (d) oxygen diffusion, and (e) total S^{ox}. Note the different scale in (d), which is 1 order of magnitude smaller than the other terms. Contours in (a)–(d) indicate the average limits of the ACC. Contours in (e) are the isopycnals at the winter ML base. The straight lines in (e) indicate the position of the sections plotted in Figure 3. The global contribution of each term is indicated on each panel's title, and the two extreme values of diffusion and the total oxygen flux are shown on top of the colorbars

The eddy-induced term (Figure 2b) plays a role in S^{ox}, especially in the North Atlantic and the Southern Ocean (Portela et al., 2020; Sallée et al., 2010). However, the main contributor to the ocean oxygenation is the vertical velocity (299 Tmol year^{-1}). This term is relatively weak but homogeneously positive over the large extension of the subtropical gyres. On the other hand, negative vertical velocity drives O^{ox} near Antarctica and in the equatorial upwelling band where it dominates the total oxygen flux.

Oxygen diffusion, as found in other studies (Kwon et al., 2016), is one order of magnitude smaller than the other terms on a regional scale, but it is not negligible in the global integral. Vertical oxygen diffusion has been thoroughly assessed in this study, but the real contribution of the lateral component is uncertain. With the choice of k_l made here, the lateral component represents two thirds of the total oxygen diffusion (Figure S5). Varying k_l over the range found in the literature would result in S^{ox} to range between −13% and +120% of its estimated value (413 Tmol year^{-1}). This suggests the important role that oxygen diffusion could pottentially play in the global oxygen uptake.

To first order, mass and properties subducted into the ocean interior spread along isopycnals and $[O_2]$ diminishes by mixing and biological consumption along the spreading path. The analysis of Apparent Oxygen Utilization (AOU = $O_{sat} - [O_2]$) sections across every ocean basin (Figure 3) can be considered as a proxy of the water mass age (a reasonable assumption around the ML base (Brandt et al., 2015)). AOU can then be used to trace water masses back to the main ventilation hot spots in a way similar to the Lagrangian approach.

Most obductive regions show relatively high AOU (Figure 3), which indicates that water has been subducted in remote locations and undergone mixing and biological consumption along its path. In the particular case of the North Atlantic, water subducted within the Subpolar Gyre in the Labrador Sea is transported into deep layers (>1,000 m) while the water that is obducted further south, downstream of the main Gyre's flow, has a different, less dense, subtropical origin (Figure 3c). However, the resolution of our computations does not allow to elucidate if the oxygen subducted in the Irminger Sea experiences further reventilation and is resubducted in the Labrador Sea (Figure S6) as suggested by McCartney (1982).

In the Indian and Pacific basins, recently subducted waters with low AOU are isopycnally transported and mixed northward (Figure 3a, 3b, and 3d). In these basins, mode waters (delimited by the two upper thick
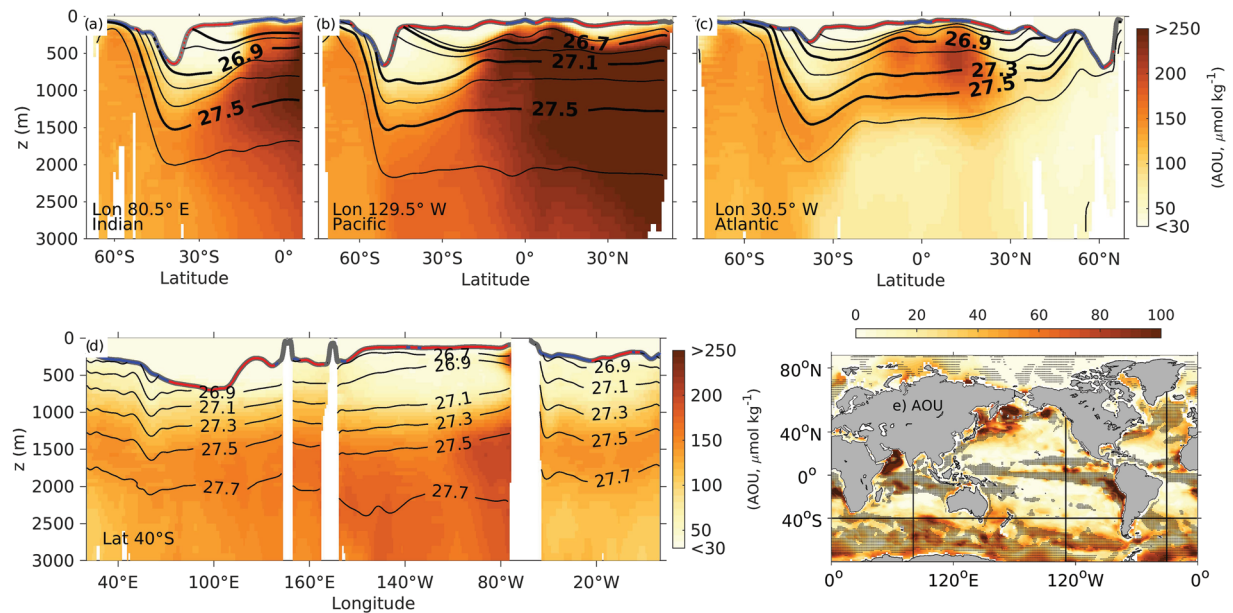
Figure 3. (a–c) Mean meridional sections of AOU across the (a) Indian, (b) Pacific, and (c) Atlantic oceans. (d) Zonal section of AOU at 40°S. Black contours in (a)–(d) represent the mean depth of the isopycnals from 26.5 to 27.7 kg m^{-3}, and the thicker lines illustrate the SAMW and AAIW limits in every basin. The thick gray contour represents the deepest ML depth, which has blue and red dots superimposed to indicate the subduction and obduction zones, respectively. (e) AOU at the late winter ML base. The stippling corresponds with obductive regions. The straight lines in (e) represent the position of the sections.

contours in Figures 3a–3c) are never reventilated, which results in increased AOU along their northward journey.

In the Southern Ocean (Figure 3d), well-oxygenated waters are subducted near Antarctica during Bottom Water formation (Marshall & Speer, 2012; Speer et al., 2000). This feature is not well captured in our S^{ox} computation (Figure 2), but it leaves its signature with a relative deep AOU minimum deeper than 2,000 m (Figures 3a–3c).

4.2. Water Mass Ventilation

The integrated effect of S^{ox} on isopycnals provides additional insight into the ocean (de)oxygenation during water mass formation and erosion. As expected, the maximum oxygen uptake in every ocean basin occurs within the Mode Waters density range (Figures 4a–4f) (Karstensen et al., 2008). Moreover, while mode waters density outcrops occupy 36% of the ML-base surface, they jointly account for 70% of the global oxygen uptake, and they are dominant in every ocean basin (Figure 4f).

The intense oxygen uptake during Subantarctic Mode Water (SAMW) subduction occurs over a narrow density range in each Southern Ocean basin (Liu & Huang, 2012; Portela et al., 2020; Sallée et al., 2010).

In the northern North Atlantic, outcropping isopycnals denser than 26.5 kg m^{-3} undergo wide meridional excursions (Luyten et al., 1985) (Figure 2d). Due to this, the strong S^{ox} detected at $\sigma = 27.8$ kg m^{-3} comprises both the Subpolar Mode Water (SPMW) and waters of the Nordic Seas, where strong deep convection and associated subduction occur (Marshall, 1999). Half of the oxygen uptake in the Southern Ocean and the North Atlantic is tied to SAMW and SPMW formation (Figure 4f), which occurs within only 22% and 15% of the global outcropping area, respectively. Hereinafter, we will refer to the ensemble of these two-mode waters as Subantarctic-Subpolar Mode Waters (SA-SPMW). This strong oxygen uptake during SA-SPMW formation is driven by lateral induction. The diffusion contribution is negligible with the reference diffusivity considered in this study, but it could be important in the SA-SPMW density range with an enhanced k_l value, as shown by the unshaded bars in Figures 4a–4e.

The second largest peak of S^{ox} corresponds to Subtropical Mode Waters (STMW). It is less intense but extends over a greater density range than SA-SPMW (Figure 4). STMW formation accounts for more than
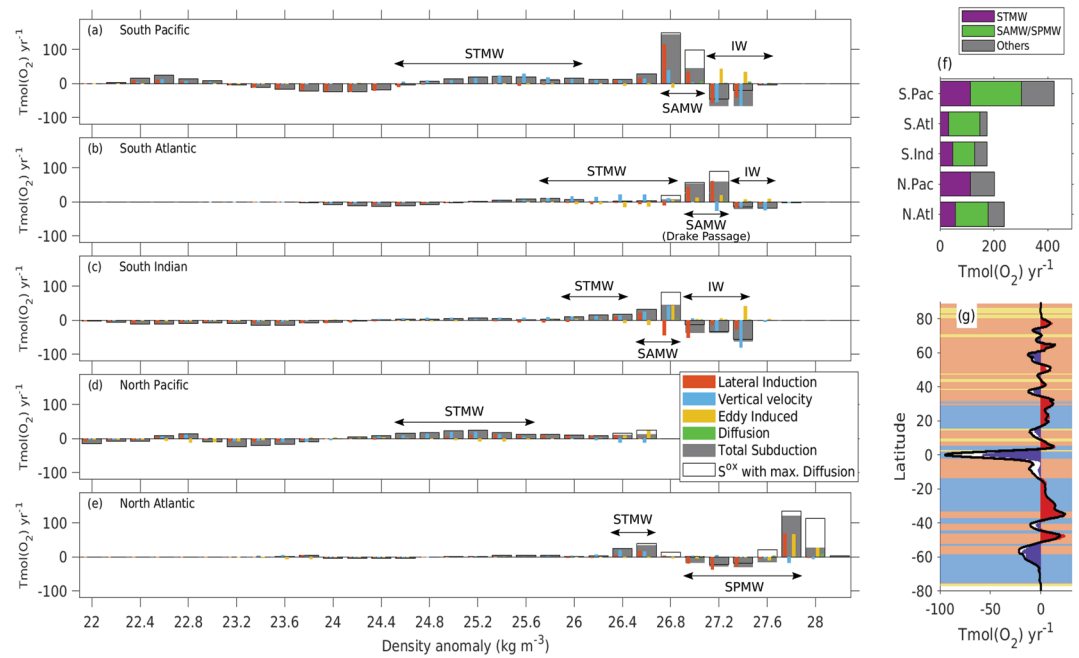
Figure 4. (a–e) Mean S^{ox} and its contributing terms by density class. (f) Contribution of the STMW and SA-SPMW to the total oxygen uptake in each basin. (g) Zonal average of kinematic oxygen subduction rates where red (blue) colors indicate net S^{ox} (O^{ox}). The solid black curve represents the zonal oxygen flux assuming a homogeneous spatial oxygen distribution (global average value). This curve demonstrates the small role that $[O_2]$ distribution plays on total S^{ox}. The background shading in (g) shows the zonally dominant subduction component. The shading colors correspond to the legend in panel (d).

half of the oxygen uptake, particularly in the North Pacific Ocean (Figure 4f). This S^{ox} is driven by the vertical velocity (background shading in Figure 4g) linked to Ekman pumping (Marshall et al., 1993; Qiu & Huang, 1995).

Maximum O^{ox} occurs (i) in the Southern Ocean, associated with the obduction mass flux that erodes AAIW (Portela et al., 2020) driven by a combination of lateral induction and wind-driven vertical flux (Figures 4a–4c); (ii) in the North Atlantic, driven by lateral induction (Figure 4e); and (iii) in the equatorial strip (Figure 2c), where the wind-driven upwelling constitutes the zonal maximum of oxygen release (Figure 4g).

The meridional distribution of $[O_2]$, with the exception of the equatorial band, has a negligible effect on global S^{ox}, which in turn is determined by the mass flux (Kwon et al., 2016). This is suggested by the small difference between S^{ox} as computed from Equation 1 (filled area in Figure 4g) and that computed by assuming spatially homogeneous $[O_2]$ (black curve).

5. Discussion and Conclusion

This study provides a thorough description and the first quantification of the physical drivers of the ocean breathing. SA-SPMW are formed in hot spots of intense lateral induction, and the wind-driven vertical velocity, although locally weak, dominates STMW subduction within the subtropical gyres. While Mode waters occupy 70% of the outcropping area at the ML base, they account for 36% of the S^{ox} during their formation process. The enhanced contribution of mode water to the oxygen injection into the ocean interior corroborates their key role in ocean oxygenation. S^{ox} is regulated by the physical mass flux while the meridional distribution of $[O_2]$ linked to the solubility effect has a minor role (Kwon et al., 2016).

Oxygen diffusion, a term often neglected (Kwon et al., 2016), is locally small, but it plays a role in the global integral. In fact, the contribution of oxygen diffusion could be underestimated here for two main reasons: (i) the value of k_l being uncertain, our choice results in an S^{ox} that is close to its lowest boundary. In

contrast, S^{ox} would be more than doubled with the maximum k_l found in the literature. (ii) Although k_v has been thoroughly assessed in this study, it only considers the tidal mixing, and it does not account for convective-driven mixing at the base of the ML during winter (Kolodziejczyk & Gaillard, 2013; Yeager & Large, 2007), so it is likely underestimated. The role of tidally driven mixing in shaping the concentration of passive tracers in the open ocean has recently been highlighted by Tuerena et al. (2019), and the negative oxygen diffusion trend was found to be the dominant contributor of the predicted ocean deoxygenation over this century (Couespel et al., 2019).

The Southern Ocean and the North Atlantic are the two lungs of the ocean. One third of the global oxygen uptake and nearly half of the oxygen release take place in the Southern Ocean. Moreover, the interbasin exchange provided by the ACC is, at least, one order of magnitude larger than all the other interbasin flows combined (Rintoul, 2000), which increases its potential to export oxygen to the rest of the ocean. The oxygen subducted in the Southern Ocean is distributed (i) to intermediate depths following SAMW formation (Hanawa & Talley, 2001; Kolodziejczyk et al., 2019; Portela et al., 2020) and (ii) to the deep ocean during the Bottom Water formation (Marshall & Speer, 2012; Rintoul, 2000; Speer et al., 2000). On the other hand, in the Northern North Atlantic, oxygen is provided to North Atlantic Deep Water through winter deep convection (Fröb et al., 2016; Körtzinger et al., 2004; Wolf et al., 2018) as part of the Atlantic Meridional Overturning Circulation (AMOC) (Lumpkin & Speer, 2007).

The strong obduction regions in the Southern Ocean have been substantially affected for deoxygenation over the past decades (Oschlies et al., 2018). This can be explained by an increase of the obduction rate and the stratification in this region. The resulting reduced ventilation leads to a progressive substitution of relatively oxygenated waters by older waters with lower $[O_2]$ (Helm et al., 2011). This, in addition to the slowdown of the AMOC over the 20th century (Rahmstorf et al., 2015), is consistent with the stronger global deoxygenation of deep waters (>1,200 m) in relation to those of surface and intermediate depths (Oschlies et al., 2018).

It is well known that subsurface primary production makes a contribution to the oxygen flux in permanent stratified regions such as the Oxygen Minimum Zones (Richardson & Bendtsen, 2017). However, globally, the physical mechanisms dominate the injection of oxygen into the ocean interior. While S^{ox} is critical for the long-term oxygen inventory, some of its components, like diffusion or eddy-induced subduction, are still uncertain and rarely assessed. The present study contributes to the understanding of ocean (de)oxygenation by providing new insight on the role of the different mechanisms driving S^{ox}. Particularly, we show that mode water distribution and the magnitude and spatial variability of diffusion must be well defined in climate models to accurately reproduce and predict oxygen variability.

The sparse historical oxygen data sets have complicated to obtain a reliable global oxygen inventory and separating natural variability from long-term climate-related trends. Ongoing deployment of the biogeochemical Argo global network including systematic oxygen measurements will bring new opportunities for investigating the drivers of global (de)oxygenation and for monitoring the temporal evolution of S^{ox} as well as the biogeochemical processes that affect the $[O_2]$.

Data Availability Statement

The data used in this study are publicly available (ECCOv4 data can be obtained in https://ecco.jpl.nasa.gov/drive/files; WOD18 oxygen data can be obtained in https://www.nodc.noaa.gov/OC5/woa18/woa18data.html). ISAS15 is produced at LOPS as part of the Service National d'Observation ArgoFrance and made is freely available (http://doi.org/10.17882/52367). The vertical diffusivity fields are available online (at https://www.seanoe.org/data/00619/73082/).

References

Abernathey, R. P., & Marshall, J. (2013). Global surface eddy diffusivities derived from satellite altimetry. *Journal of Geophysical Research: Oceans*, *118*, 901–916. https://doi.org/10.1002/jgrc.20066

Bopp, L., Le Quéré, C., Heimann, M., Manning, A. C., & Monfray, P. (2002). Climate-induced oceanic oxygen fluxes: Implications for the contemporary carbon budget. *Global Biogeochemical Cycles*, *16*(2), 6–1–6–13. https://doi.org/10.1029/2001gb001445

Bopp, L., Resplandy, L., Orr, J. C., Doney, S. C., Dunne, J. P., Gehlen, M., et al. (2013). Multiple stressors of ocean ecosystems in the 21st century: Projections with CMIP5 models. *Biogeosciences*, *10*(10), 6225–6245. https://doi.org/10.5194/bg-10-6225-2013

Brandt, P., Bange, H. W., Banyte, D., Dengler, M., Didwischus, S. H., Fischer, T., et al. (2015). On the role of circulation and mixing in the ventilation of oxygen minimum zones with a focus on the eastern tropical North Atlantic. *Biogeosciences*, *12*(2), 489–512. https://doi.org/10.5194/bg-12-489-2015

Couespel, D., Marina, L., & Bopp, L. (2019). Major contribution of reduced upper ocean oxygen mixing to global ocean deoxygenation in an Earth System Model. *Geophysical Research Letters*, *46*, 12,239–12,249. https://doi.org/10.1029/2019GL084162

Cushman-Roisin, B. (1987). Subduction. In P. Muller & D. Henderson (Eds.), *Dynamics of the oceanic mixed layer*, *Hawaii Institute of Geophysics Special Publication* (pp. 81–196). Honolulu, HI: Univ. of Hawaii.

de Lavergne, C., Vic, C., Madec, G., Roquet, F., Waterhouse, A. F., Whalen, C. B., et al. (2020). A parameterization of local and remote tidal mixing. *Journal of Advances in Modeling Earth Systems*, *12*, e2020MS002065. https://doi.org/10.1029/2020ms002065

Donners, J., Drijfhout, S. S., & Hazeleger, W. (2005). Water mass transformation and subduction in the South Atlantic. *Journal of Physical Oceanography*, *35*(10), 1841–1860. https://doi.org/10.1175/JPO2782.1

Forget, G., Ferreira, D., & Liang, X. (2015). On the observability of turbulent transport rates by Argo: Supporting evidence from an inversion experiment. *Ocean Science*, *11*(5), 839–853. https://doi.org/10.5194/os-11-839-2015

Fröb, F., Olsen, A., Våge, K., Moore, G. W. K., Yashayaev, I., Jeansson, E., & Rajasakaren, B. (2016). Irminger Sea deep convection injects oxygen and anthropogenic carbon to the ocean interior. *Nature Communications*, *7*, 13244. https://doi.org/10.1038/ncomms13244

Fukumori, I., Wang, O., Fenty, I., Forget, G., Heimbach, P., & Ponte, R. M. (2017). ECCO Version 4 Release 3. *Dspace.Mit.Edu*, *2*(2015), 10. https://hdl.handle.net/1721.1/110380

Gaillard, F., Reynaud, T., Thierry, V., Kolodziejczyk, N., & Von Schuckmann, K. (2016). In situ-based reanalysis of the global ocean temperature and salinity with ISAS: Variability of the heat content and steric height. *Journal of Climate*, *29*(4), 1305–1323. https://doi.org/10.1175/JCLI-D-15-0028.1

Garcia, H. E., Weathers, K. W., Paver, C. R., Smolyar, I., Boyer, T. P., Locarnini, R. A., et al. (2019). WORLD OCEAN ATLAS 2018 Volume 3: Dissolved oxygen, apparent oxygen utilization, and dissolved oxygen saturation. *NOAA Atlas NESDIS 83*, *3*, 38.

Gent, P. R., & McWilliams, J. C. (1990). Isopycnal mixing in ocean circulation models. *Journal of Physical Oceanography*, *20*, 150–155. https://doi.org/10.1175/1520-0485(1990)020<0150:IMIOCM>2.0.CO;2

Gruber, N., Gloor, M., Fan, S. M., & Sarmiento, J. L. (2001). Air-sea flux of oxygen estimated from bulk data: Implications for the marine and atmospheric oxygen cycles. *Global Biogeochemical Cycles*, *15*(4), 783–803. https://doi.org/10.1029/2000GB001302

Hanawa, K., & Talley, L. D. (2001). Mode waters. In *Ocean circulation and climate: Observing and modeling the global ocean*, *International Geophysics Series* (Vol. 77, pp. 373–386). ftp://bslictb.nerc-bas.ac.uk/jbsall/Papers_CMIP5team/2001Hanawa.pdf

Helm, K. P., Bindoff, N. L., & Church, J. A. (2011). Observed decreases in oxygen content of the global ocean. *Geophysical Research Letters*, *38*, 1–6. https://doi.org/10.1029/2011GL049513

Ito, T., Minobe, S., Long, M. C., & Deutsch, C. (2017). Upper ocean O$_2$ trends: 1958–2015. *Geophysical Research Letters*, *44*, 4214–4223. https://doi.org/10.1002/2017gl073613

Joos, F., Platiner, G. K., Stocker, T. F., Kortzinger, A., & Wallace, D. W. R. (2003). Trends in marine dissolved oxygen: Implications for ocean circulation changes and the carbon budget. *Eos*, *84*(21), 84–86. https://doi.org/10.1029/2003EO210001

Karstensen, J., Stramma, L., & Visbeck, M. (2008). Oxygen minimum zones in the eastern tropical Atlantic and Pacific oceans. *Progress in Oceanography*, *77*(4), 331–350. https://doi.org/10.1016/j.pocean.2007.05.009

Keeling, R. F., & Garcia, H. E. (2002). The change in oceanic O$_2$ inventory associated with recent global warming. *Proceedings of the National Academy of Sciences of the United States of America*, *99*(12), 7848–7853. https://doi.org/10.1073/pnas.122154899

Keeling, R. F., Körtzinger, A., & Gruber, N. (2010). Ocean deoxygenation in a warming world. *Annual Review of Marine Science*, *2*(1), 199–229. https://doi.org/10.1146/annurev.marine.010908.163855

Klocker, A., & Abernathey, R. (2014). Global patterns of mesoscale eddy properties and diffusivities. *Journal of Physical Oceanography*, *44*(3), 1030–1046. https://doi.org/10.1146/annurev.marine.010908.163855

Koelling, J., Wallace, D. W. R., Send, U., & Karstensen, J. (2017). Intense oceanic uptake of oxygen during 2014–2015 winter convection in the Labrador Sea. *Geophysical Research Letters*, *44*, 7855–7864. https://doi.org/10.1002/2017GL073933

Köhl, A., Stammer, D., & Cornuelle, B. (2007). Interannual to decadal changes in the ECCO global synthesis. *Journal of Physical Oceanography*, *37*(2), 313–337. https://doi.org/10.1175/JPO3014.1

Kolodziejczyk, N., & Gaillard, F. (2013). Variability of the heat and salt budget in the subtropical southeastern Pacific mixed layer between 2004 and 2010: Spice injection mechanism. *Journal of Physical Oceanography*, *43*(9), 1880–1898. https://doi.org/10.1175/JPO-D-13-04.1

Kolodziejczyk, N., Llovel, W., & Portela, E. (2019). Interannual variability of upper ocean water masses as inferred from Argo Array. *Journal of Geophysical Research: Oceans*, *124*, 6067–6085. https://doi.org/10.1029/2018JC014866

Kolodziejczyk, N., Prigent-Mazella, A., & Gaillard, F. (2017). ISAS-15 temperature and salinity gridded fields. SEANOE. https://doi.org/10.17882/52367

Körtzinger, A., Schimanski, J., Send, U., & Wallace, D. (2004). The ocean takes a deep breath. *Science*, *306*(5700), 1337. https://doi.org/10.1126/science.1102557

Kwon, E. Y., Deutsch, C., Xie, S. P., Schmidtko, S., & Cho, Y. K. (2016). The North Pacific oxygen uptake rates over the past half century. *Journal of Climate*, *29*(1), 61–76. https://doi.org/10.1175/JCLI-D-14-00157.1

Liu, L. L., & Huang, R. X. (2012). The global subduction/obduction rates: Their interannual and decadal variability. *Journal of Climate*, *25*(4), 1096–1115. https://doi.org/10.1175/2011JCLI4228.1

Long, M. C., Deutsch, C., & Ito, T. (2016). Finding forced trends in oceanic oxygen. *Global Biogeochemical Cycles*, *30*(2), 381–397. https://doi.org/10.1002/2015GB005310

Lumpkin, R., & Speer, K. (2007). Global ocean meridional overturning. *Journal of Physical Oceanography*, *37*(10), 2550–2562. https://doi.org/10.1175/JPO3130.1

Luyten, J., Pedlosky, J., & Stommel, H. (1983). The ventilated thermocline. *Journal of Physical Oceanography*, *13*, 292–309. https://doi.org/10.1007/BF02423489

Luyten, J., Stommel, H., & Wunsch, C. (1985). A diagnostic study of the Northern Atlantic Subpolar Gyre. *Journal of Physical Oceanography*, *15*, 1344–1348. https://doi.org/10.1175/1520-0485(1985)015<1344:ADSOTN>2.0.CO;2

Marshall, J. (1999). OPEN-OCEAN convection: Observations, theory, and models. *Reviews of Geophysics*, *37*(1), 1–64.

Marshall, J., & Speer, K. (2012). Closure of the meridional overturning circulation through Southern Ocean upwelling. *Nature Geoscience*, *5*(3), 171–180. https://doi.org/10.1038/ngeo1391

Marshall, J. C., Williams, R. G., & Nurser, A. J. G. (1993). Inferring the subduction rate and period over the North Atlantic. *Journal of Physical Oceanography*, *23*, 1315–1329. https://doi.org/10.1175/1520-0485(1993)023<1315:ITSRAP>2.0.CO;2

McCartney, M. S. (1982). The subtropical recirculation of mode waters. Reprint from Journal of Marine Research. Vol. 40 (No. Supplement). Retrieved from http://www.whoi.edu/science/PO/people/mmccartney/pdfs/McCartney82.pdf

Munk, W., & Wunsch, C. (1998). Abyssal recipes II: Energetics of tidal and wind mixing. *Deep-Sea Research Part I: Oceanographic Research Papers*, *45*(12), 1977–2010. https://doi.org/10.1016/S0967-0637(98)00070-3

Naveira Garabato, A. C. N., MacGilchrist, G. A., Brown, P. J., Evans, D. G., Meijers, A. J. S., & Zika, J. D. (2017). High-latitude ocean ventilation and its role in Earth's climate transitions. *Philosophical Transactions of the Royal Society A: Mathematical, Physical and Engineering Sciences*, *375*(2102), 20160324. https://doi.org/10.1098/rsta.2016.0324

Osborn, T. R. (1980). Estimates of the local rate of vertical diffusion from dissipation measurements. *Journal of Physical Oceanography*, *10*, 83–89.

Oschlies, A., Brandt, P., Stramma, L., & Schmidtko, S. (2018). Drivers and mechanisms of ocean deoxygenation. *Nature Geoscience*, *11*(7), 467–473. https://doi.org/10.1038/s41561-018-0152-2

Portela, E., Kolodziejczyk, N., Maes, C., & Thierry, V. (2020). Interior water-mass variability in the Southern Hemisphere oceans during the last decade. *Journal of Physical Oceanography*, *50*(2), 361–381. https://doi.org/10.1175/JPO-D-19-0128.1

Qiu, B., & Huang, R. X. (1995). Ventilation of the North Atlantic and North Pacific: Subduction versus obduction. *Journal of Physical Oceanography*, *25*, 2374–2390. https://doi.org/10.1175/1520-0485(1995)025<2374:VOTNAA>2.0.CO;2

Rahmstorf, S., Box, J. E., Feulner, G., Mann, M. E., Robinson, A., Rutherford, S., & Schaffernicht, E. J. (2015). Exceptional twentieth-century slowdown in Atlantic Ocean overturning circulation. *Nature Climate Change*, *5*(5), 475–480. https://doi.org/10.1038/nclimate2554

Resplandy, L. (2018). Climate change and oxygen in the ocean. *Nature*, *557*, 314–315. https://doi.org/10.1038/nature15216

Richardson, K., & Bendtsen, J. (2017). Photosynthetic oxygen production in a warmer ocean: The Sargasso Sea as a case study. *Philosophical Transactions of the Royal Society A: Mathematical, Physical and Engineering Sciences*, *375*(2102), 375. https://doi.org/10.1098/rsta.2016.0329

Rintoul, S. R. (2000). Southern Ocean currents and climate. *Papers and Proceedings of the Royal Society of Tasmania*, *133*(3), 41–50. https://doi.org/10.26749/rstpp.133.3.41

Sallée, J. B., Matear, R. J., Rintoul, S. R., & Lenton, A. (2012). Localized subduction of anthropogenic carbon dioxide in the Southern Hemisphere oceans. *Nature Geoscience*, *5*(8), 579–584. https://doi.org/10.1038/ngeo1523

Sallée, J.-B., Speer, K., Rintoul, S., & Wijffels, S. (2010). Southern Ocean thermocline ventilation. *Journal of Physical Oceanography*, *40*(3), 509–529. https://doi.org/10.1175/2009JPO4291.1

Schmidtko, S., Stramma, L., & Visbeck, M. (2017). Decline in global oceanic oxygen content during the past five decades. *Nature*, *542*(7641), 335–339. https://doi.org/10.1038/nature21399

Speer, K., Rintoul, S. R., & Sloyan, B. (2000). The diabatic Deacon cell* *Journal of Physical Oceanography*, *30*(12), 3212–3222. https://doi.org/10.1175/1520-0485(2000)030<3212:tddc>2.0.co;2

Stramma, L., Johnson, G. C., Sprintall, J., & Mohrholz, V. (2008). Expanding oxygen-minimum zones in the tropical oceans. *Science*, *320*(5876), 655–658. https://doi.org/10.1126/science.1153847

Tuerena, R. E., Williams, R. G., Mahaffey, C., Vic, C., Green, J. A. M., Naveira-Garabato, A., et al. (2019). Internal tides drive nutrient fluxes into the deep chlorophyll maximum over mid-ocean ridges. *Global Biogeochemical Cycles*, *33*(8), 995–1009. https://doi.org/10.1029/2019GB006214

Wolf, M. K., Hamme, R. C., Gilbert, D., Yashayaev, I., & Thierry, V. (2018). Oxygen saturation surrounding deep water formation events in the Labrador Sea from Argo-O2 data. *Global Biogeochemical Cycles*, *32*(4), 635–653. https://doi.org/10.1002/2017GB005829

Wyrtki, K. (1965). Surface Currents of the Eastern Tropical Pacific Ocean. *Inter-American Tropical Tuna Comission*, *9*(5), 271–304.

Yeager, S. G., & Large, W. G. (2007). Observational evidence of winter spice injection. *Journal of Physical Oceanography*, *37*(12), 2895–2919. https://doi.org/10.1175/2007JPO3629.1